Scripta Materialia 258 (2025) 116509

Contents lists available at ScienceDirect

Scripta Materialia

journal homepage: www.journals.elsevier.com/scripta-materialia

Evaluating neon ions as an alternative to gallium in micro cantilevers fracture testing

Eloho Okotete [a], Stefan Mück [a,b], Subin Lee [a,*], Christoph Kirchlechner [a]

[a] Institute for Applied Materials, Karlsruhe Institute of Technology, D-76131 Karlsruhe, Germany
[b] Karlsruhe Nano Micro Facility (KNMFi), Karlsruhe Institute of Technology, D-76344, Eggenstein-Leopoldshafen, Germany

ARTICLE INFO

Keywords:
Crack arrest
Neon ions
FIB artefacts
Micro cantilevers
Fracture toughness

ABSTRACT

The influence of neon ions at the notch front as well as of annealing heat treatments on the fracture toughness of single crystalline silicon was investigated via microcantilever fracture testing. Using in situ scanning electron microscope deformation, the fracture toughness of the neon-notched cantilevers after annealing was measured, resulting in an average value of 1.0 MPa $m^{0.5}$, proving that chemically inert gas ions can result in similar fracture toughness values as with Ga FIBs. However, Ne bubble formation was identified as substantial source of errors and we advise caution when interpreting fracture toughness measurements when using Ne as chemically inert ion species for notching.

In micro fracture studies, gallium focused ion beam (FIB) has been widely used to fabricate specimens such as micro cantilevers and their notches. The influence of gallium ion-induced artefacts surrounding the FIB-notch is a subject of on-going debate [1–6], particularly in material systems prone to brittle fracture, where unstable fracture often initiates from the notch. While crack arrest before unstable fracture through the bridge-notch geometry has been suggested to reduce the impact of these artefacts in hard coatings [7] and single crystal silicon [8,9], the chemical interactions between Ga^+ and the test material have not been thoroughly addressed. Gallium is known to form secondary phases with copper [10], and segregate to grain boundaries in selected materials, specifically aluminium, leading to liquid metal embrittlement [11–13], which significantly alters fracture behaviour. This underscores the need for alternative approaches to notching cantilevers.

Alternative ion species have been sparsely examined to replace Ga^+ for preparing notches in micro fracture experiments. For instance, Best et al. [14] used He^+, Xe^+ and Ga^+ ions to create notches for fracture studies of CrN hard coatings using micro cantilever geometry. The study reported that fracture toughness measured from the inert ion-notched cantilevers was generally lower than that from Ga^+ notched samples. However, the reason for higher fracture toughness values in the He^+ notched samples with a notch radius of 35–50 nm compared to Xe^+ notched ones with a notch radius of 100–110 nm was not identified by the authors. Additionally, this study showed that creating deep notches is challenging due to the low sputtering yield of He^+ and swelling effects observed at high ion acceleration voltage. Preiß et al. [15] also used Ne^+, Xe^+ and Ga^+sources to create slits in gold membranes for bulge testing. No clear influence of the notching ions or notch radius on the fracture toughness was reported, which was attributed to the true thickness slits milled on the polycrystalline membranes. Although these studies highlight the promise of using alternative ions for notching in small-scale fracture studies, the direct influence of these potential alternative ions on micro fracture studies has not been extensively discussed till date. Therefore, a detailed analysis of the role of alternative notching ions on measured fracture toughness from micro cantilever-based studies is of considerable interest within the community.

The aim of this study is to investigate the fracture properties of silicon cantilevers with a bridge notch fabricated using noble gas ions, specifically Ne^+ ions. The following sections present the steps taken to optimise milling conditions for notch fabrication using neon gas field ion sources (GFIS). Thereafter, the fracture toughness of the neon-notched micro cantilever is calculated and analysed.

Single crystal silicon is chosen as a model material to study the role of ion species on the fracture toughness of small components for two major reasons. First, silicon plays a crucial role in the semiconductor industry [16,17], and therefore has been the subject of many fracture studies to ensure the reliability of micro-electro-mechanical systems (MEMS) components in service. In addition, the effects of FIB-artefacts, such as notch root radius, stress state, and impurities at the notch on the fracture of single crystalline micro cantilevers, have received minimal attention

* Corresponding author.
E-mail address: subin.lee@kit.edu (S. Lee).

https://doi.org/10.1016/j.scriptamat.2024.116509
Received 28 October 2024; Received in revised form 9 December 2024; Accepted 9 December 2024
Available online 16 December 2024

till now. Hence, single crystalline silicon is notched in this study using Ne^+ GFIS with small ion probe size [18–20] and ion beam tails [21]. The high resolution of the GFIS arises from emission of ions from a single atom at the emitter [19,22]. Neon is preferred over helium for this investigation because of its high sputter yield (~20 times higher) and less damage depth (~5 times less than helium, based on penetration depth calculation from simulations) in silicon [23–25].

Free-standing cantilevers were fabricated on a (110) silicon on insulator (SOI) wafer (Siegert GmbH, Germany). A combination of electron beam lithography and reactive ion etching was used to prepare the cantilevers. Details of the fabrication process can be found in [8,9]. The cantilevers had nominal a width and thickness between 2 and 2.5 μm, a length maintained at 5 times the thickness, and a notch depth (a/W) of approximately 0.35. Line notches were milled using a helium ion microscope (HIM) equipped with a neon GFIS (Orion Nanofab, Carl Zeiss AG, Germany). A neon gas pressure of 7.3×10^{-6} mbar was maintained at the source for the generation of the ion beam, and the acceleration voltages of 10, 15, and 25 kV were used. The final milling currents were between 10 and 20 pA, achieved by a 20 μm diameter aperture and varying spot control. Nanopatterning visualization engine (NPVE) was used to mill the line patterns at doses of 1 nC/μm and a dwell time of 1 μs. After notching, selected samples were annealed in a vacuum of 2.9×10^{-5} mbar at 450 °C for 1 h and at 750 °C for 1.5 h in a quartz tube within a tubular furnace. All the notched micro cantilevers were tested in situ using a PI 89 indenter (Hysitron, Bruker, USA) with a 10 μm wedge tip (Synton-MDP AG, Switzerland) inside a scanning electron microscope (SEM, Merlin, Carl Zeiss AG, Germany). Displacement-controlled loading at a displacement rate of 10 nm/s was used.

Cantilevers with bridge notches exhibit typical linear elastic fracture behaviour, as illustrated by a representative load-displacement curve shown in Fig. 1. A total of 65 cantilevers was tested under varying ion acceleration voltages, specifically 19, 23, and 23 cantilevers notched at 25 kV, 15 kV and 10 kV, respectively. During testing, one or two small load drops were detected in 30 cantilevers, similar to the observations in Ga^+ bridge-notched cantilevers [7–9], indicating failures of the bridges. The force at these load drops denoted as F_{B1}, F_{B2}, and F_C represents the maximum load at the material bridges and final fracture, respectively. This observation suggests that the natural crack from the failure of the material bridges arrests before the final fracture [7]. After bridge failure, a through-thickness notch was assumed for calculating the fracture toughness. The fracture toughness (K_{IC}) at the through-thickness notch

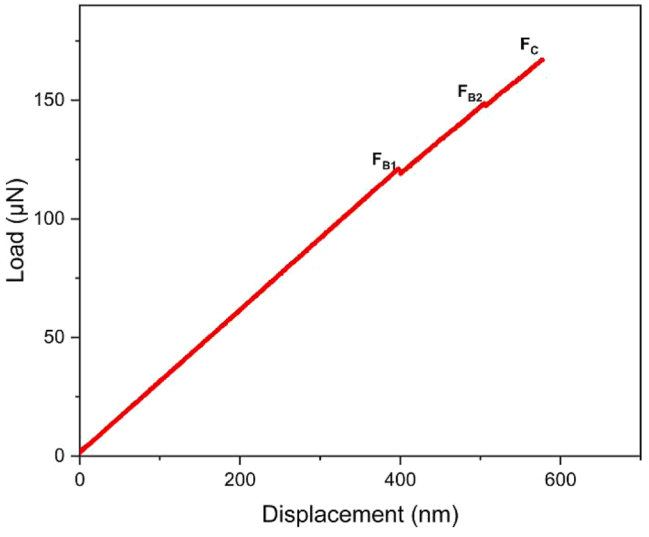

Fig. 1. A representative load-displacement plot of a neon ion bridge-notched silicon cantilever showing crack arrest. Two distinctive load drops due to bridge failure were observed prior to the final fracture of the cantilever.

and the bridge notch fracture toughness (K_{IC}*) was calculated for cantilevers where crack arrest was observed using Eqs. (1) [26] and (2) [27],

$$K_{IC} = \frac{F_C L}{BW^{3/2}} f_{Matoy}\left(\frac{a}{W}\right) \tag{1}$$

$$f_{Matoy}\left(\frac{a}{W}\right) = 1.46 + 24.36\left(\frac{a}{W}\right) - 47.21\left(\frac{a}{W}\right)^2 + 75.18\left(\frac{a}{W}\right)^3$$

$$K^*_{IC} = \frac{F_B L}{BW^{3/2}} f_{Matoy}\left(\frac{a}{W}\right)\frac{1}{f_{corr}} \tag{2}$$

where F_B is the load at bridge failures; L, B, and W are the length, width, and thickness of the cantilever; a is the notch length; f_{Matoy} is a geometry correction factor; and f_{corr} is a bridge notch correction factor. The correction factor, f_{corr} is derived from FEM simulations [27] and depends on the geometry of the notch and the bridge. It quantifies the relationship between the stress intensity factor at the top half of the bridge and that at the notch front, enabling the calculation of the apparent fracture toughness based on bridge failure. When crack arrest was not observed during the experiments (i.e., no load drops), an apparent fracture toughness was used for the analysis. A conditional fracture toughness (K_{IQ}) replaces K_{IC} in Eq. (1), and then it was corrected for the influence of bridge notch geometry using Eq. (3) [27].

$$K_{IQ_{corrected}} = \frac{K_{IQ}}{f_{corr}} \tag{3}$$

To achieve a high sputter yield for sharp and deep notches, the acceleration voltage was optimized. SEM images (Fig. 2(a)–(c)) show that the width of the milled notches increases as the acceleration voltage decreases. At 25 kV (Fig. 2c), the notch exhibits the narrowest width (95 nm) compared to the others prepared by lower ion energies, potentially indicating a small notch root radius. This is attributed to the increase in beam probe size at lower acceleration voltages resulting from chromatic aberrations [28–30]. The effect of the notch width on fracture toughness is presented in Fig. 2(d) for samples where crack arrest was present. The notch with the smallest width (milled at 25 kV) exhibited the highest average K_{IC}* and K_{IC} values, measuring 1.4 ± 0.2 MPa $m^{0.5}$ and 1.6 ± 0.2 MPa $m^{0.5}$, respectively, with the scatter representing the standard deviation. At 15 kV and 10 kV, the average K_{IC}* decreased to 1.3 ± 0.1 MPa $m^{0.5}$ for both voltages, while the average K_{IC} was 1.3 ± 0.2 MPa $m^{0.5}$ and 1.4 ± 0.3 MPa $m^{0.5}$, respectively. It should be noted that, in all cases, the measured K_{IC} values were higher than those reported for Ga^+ notched cantilevers (green data points in Fig. 2(d)) [9], which may be attributed to potential artefacts introduced by neon ions at the notch. A summary of the average fracture toughness and apparent fracture toughness for all tested samples is presented in Table 1, with further details on samples that did not exhibit crack arrest (K_{IQ} and $K_{IQ\_corrected}$) provided in Supplementary material Fig. S1.

Postmortem SEM images of the fractured samples notched with different acceleration voltages are presented in Fig. 3. Contrary to expectations, the sputter yield of silicon using neon ions decreases with increasing ion beam energy, as evidenced by the reduced notch depth at the same dose. This behaviour contrasts expectations for heavier ion species, such as Ga^+, where sputter yield typically increases with higher beam energy, though it can decline at very high impact energies. It is well established that high energy incident ions interact with the target material via electronic and nuclear collision [31–33], leading to multiple events that culminate in sputtering. The efficiency of sputtering depends on the mass of the incident ion, the mass of the target, and the energy of the incident ion [34]. Simulations such as transport of ions in matter (TRIM) and stopping and range of ions in matter (SRIM) have shown that the sputter yield of silicon with neon ions peaks at 10 kV [24, 32,35]. Beyond this energy, the implantation depth of the ions increases—simulations show a 50 % increase in neon ion implantation depth when the acceleration voltage is increased from 10 to 20 kV [24]—and

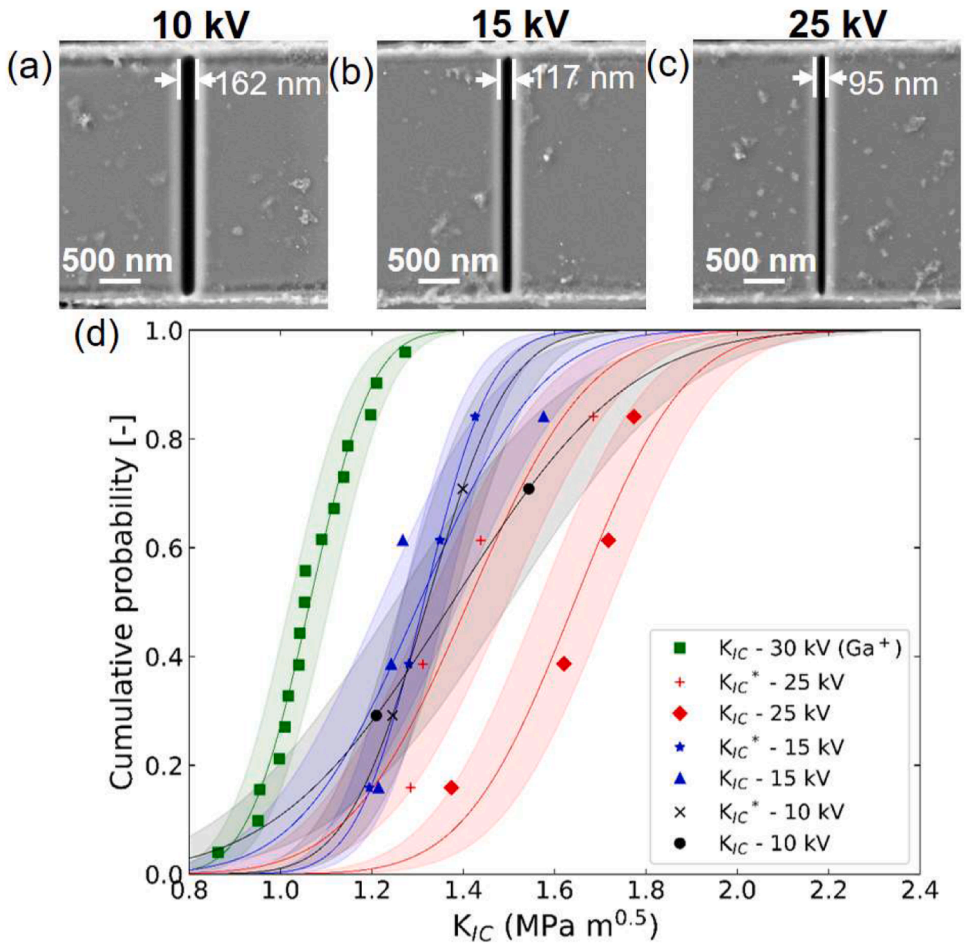

Fig. 2. SEM images showing the top view of notches milled at ion beam acceleration voltages of (a) 10 kV, (b) 15 kV and (c) 25 kV. (d) Cumulative probability distribution of through-thickness fracture toughness and bridge fracture toughness of silicon cantilevers notched with different acceleration voltage compared with Ga^+ notched cantilevers [8,9].

Table 1
Average fracture toughness measured at bridge failure and the final fracture for samples where crack arrest was present. For those crack arrest was not absent, the averaged K_{IQ} and corrected K_{IQ} are summarized. The errors represent the standard deviation.

Acceleration voltage (kV)	Crack arrest			
	Observed		Not observed	
	K_{IC}* (MPa $m^{0.5}$)	K_{IC} (MPa $m^{0.5}$)	K_{IQ} (MPa $m^{0.5}$)	$K_{IQ,corrected}$ (MPa $m^{0.5}$)
10	1.3 ± 0.1	1.4 ± 0.3	1.7 ± 0.3	1.9 ± 0.4
15	1.3 ± 0.1	1.3 ± 0.2	1.4 ± 0.2	1.5 ± 0.2
25	1.4 ± 0.1	1.6 ± 0.2	1.3 ± 0.1	1.5 ± 0.2

the nature of the ion-target interaction shifts from majorly nuclear collisions at the surface to sub-surface interactions [24,32].

This aligns with our experimental results (see Fig. 3), where higher sputter yield and reduced sub-surface damage were observed at 10 kV compared to 25 kV. At Ne ion energies below 10 kV, the milling time for notches increases significantly, leading to blunt and shallow notches that are unsuitable for reliable small scale fracture testing. On the contrary, the sub-surface interactions at 25 kV lead to bubble formation, visible in SEM images and referred to as artefacts in the following discussion.

Furthermore, Fig. 3 shows that the notch front of cantilevers milled with 25 kV Ne^+ ions is not straight but rather exhibits a rough topography. This roughness is consequence of a sub-surface gas bubble formation caused by the implantation of neon in silicon at high doses [24,36,37]. The thickness of the bubble region also increases with the acceleration voltage of the notching ion. In silicon, the sub-surface structures, which are influenced by dose, dose rate and incident energies [38,39], consist of amorphous and bubble layers [24,40–42]. Bubbles initially form due to agglomeration of the insoluble inert gas atoms at vacancies, as they seek to minimise the system's energy, followed by their growth through the absorption of other bubble nuclei or gas atoms [41,43–45]. As defect accumulation continues in the target the material, it becomes more amorphous [41,46]. These defects are also observed in the notched region of the silicon cantilevers in this study (Fig. 3) due to the high dose required to achieve deep notches.

Thermal annealing is one approach to mitigate milling artefacts from FIB-milled samples. However, such thermal treatments have also been reported to cause noticeable instability in gas-filled bubbles formed by ion implantation [37,45,47,48]. Annealing temperatures were selected to exceed the reported bubble instability threshold for inert gas–implanted single-crystal silicon substrates. This approach aimed to promote bubble growth and induce instability, thereby enabling the release of trapped Ne gas through the surface and relieving internal compressive stress caused by Ne implantation within the substrate [37,45,47]. In Fig. 4, *postmortem* SEM images of cantilevers fractured before and after annealing are presented for samples notched with ions accelerated at different voltages. No noticeable change is observed between the SEM images before (Fig. 4(a)–(c)) and after annealing at 450 °C (Fig. 4(d)–(f)). However, a porous-like structure becomes visible in the *postmortem* SEM images of the samples annealed at 750 °C, as shown in

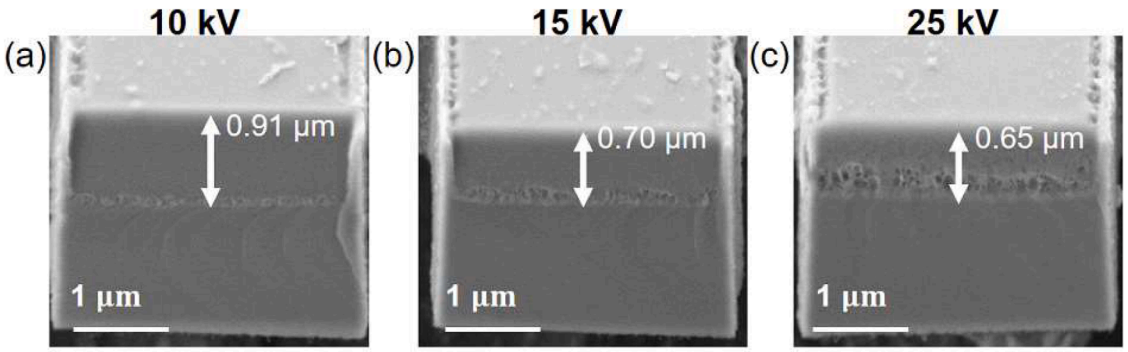

Fig. 3. Fracture cross-section of cantilevers milled with beam energies (a) 10 kV, (b) 15 kV and (c) 25 kV beam energies, and constant dose of 1 nC/µm. Higher acceleration voltage resulted in shallower notches and the formation of damage layers, such as bubble layer, at the notch front.

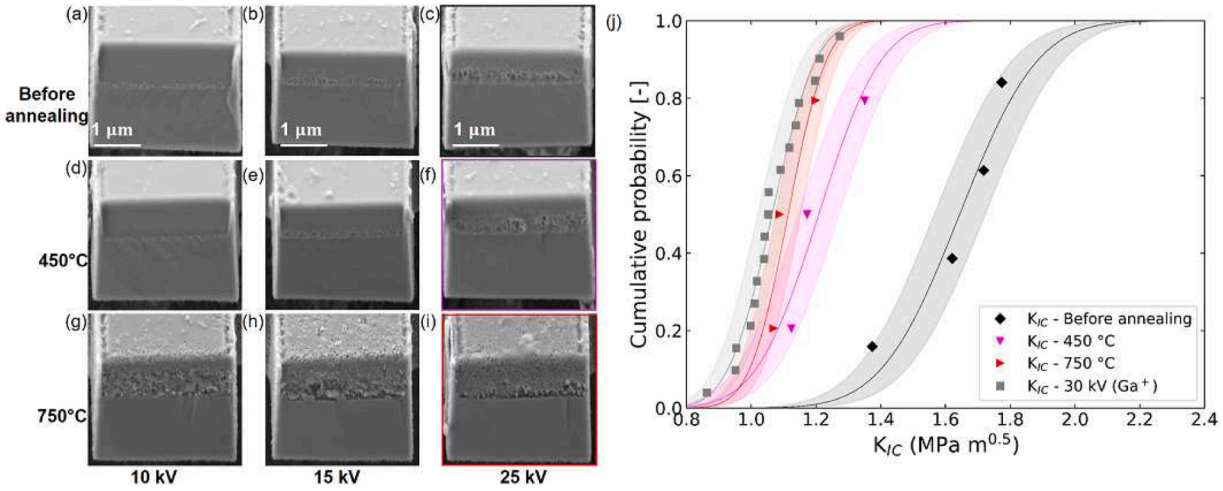

Fig. 4. Fracture cross-section of cantilevers notched using different acceleration voltages before annealing (a–c), after annealing at 450 °C (d-f) and 750 °C (g–i). Cumulative probability distribution of through-thickness fracture of toughness after annealing is seen in (j), also showing inserts of Ga^+ notched samples from [8,9].

Fig. 4(g)–(i). This structure can be described as a distribution of empty cavities with a clean and well-defined notch front observed in all the samples, suggesting the release of trapped neon in this region.

The fracture toughness of samples notched at 25 kV is compared before and after annealing (Fig. 4(j)). A clear shift in the cumulative distribution curve toward lower K_{IC} values is observed following annealing at both temperatures. The average K_{IC} reduced to 1.2 ± 0.2 MPa $m^{0.5}$ and 1.1 ± 0.1 MPa $m^{0.5}$ after annealing at 450 °C and 750 °C, respectively, compared to 1.6 ± 0.2 MPa $m^{0.5}$ before annealing. These results suggest that both annealing temperatures are potentially effective in reducing the influence from artefacts originating from neon ion-silicon interaction, despite the absence of visual changes in the *post-mortem* SEM image of samples annealed at 450 °C (compare Fig. 4(f) and (i)).

The annihilation of neon ion-induced defects after thermal annealing has been attributed to both epitaxial recrystallization of the amorphous layer and breaking/collapse of the gas-filled bubbles, leading to the ejection of neon gas [49–52]. The collapse of gas-filled bubbles is reported to occur after the bubble grow to a critical size during high temperature annealing, leaving behind cavities and voids following gas release [47,48,53]. In this study, the fractured samples after annealing show features similar to cavities described in other works where neon gas-filled bubbles were subjected to thermal treatment. The notch plane in Fig. 4 reveals numerous voids after annealing alongside a sharp crack front with cavities, indicating bubbles collapse in this region. It is likely that recrystallization of the amorphous silicon layer is suppressed during annealing because the high concentration of inert gas bubbles at interfaces leads to bonding errors [37]. It is also noteworthy that thermal treatment of neon-notched silicon samples did not lead to surface changes, unlike in gallium-notched silicon samples where Ga droplets formed on the surface after high temperature exposure [54].

The use of a GFIS for notching on lithography-fabricated silicon cantilevers eliminates chemical interactions and segregation at the notch. However, another artefact at the notch affects the measured fracture toughness. The fracture toughness of as-fabricated cantilevers at the through-thickness notch (K_{IC}) after crack arrest is about 40–60 % higher than the expected fracture toughness value of 1.0 MPa $m^{0.5}$ for single crystalline silicon (Table 1). This apparent toughening of silicon can be attributed to compressive residual stresses at the notch due to the presence of bubbles at the notch front even after crack arrest (see Fig. 3). However, it is observed that the fracture toughness at the bridge (K_{IC}*) was lower than at the through-thickness notch, which is attributed to the reduce presence of bubbles at the bridge. This indicates that fracture data from the bridges provides additional data with reduced neon bubble influence.

Thermal treatment of the notches results in an average fracture toughness of 1.1 ± 0.1 MPa $m^{0.5}$, which aligns with values calculated for the (111) silicon cleavage planes in bulk scale experiments (0.65–1.0 MPa $m^{0.5}$) [55–60] and gallium notched micro fracture studies (1.1 ± 0.1 MPa $m^{0.5}$) [8,9,61,62]. These results highlight the necessity of post-annealing to achieve accurate and reliable measurements of fracture toughness when Ne ion are used for notching cantilevers. While Ne ions exhibit no chemical interaction with silicon, they may not be ideal for creating precise notches in silicon due to bubble formation at the

notch without annealing.

However, the density and damage layer thickness are material-dependent. As an example, ion trajectory simulations using TRIM indicate that a 20 kV neon ion beam creates approximately 110 subsurface vacancies per sputtered atom in copper while about 435 vacancies per sputtered atom in silicon [63]. This significant difference suggests that, under the same implantation conditions, silicon produces a much higher concentration of vacancies than copper, which can serve as nucleation sites for neon ions to form gas bubbles; in other words, the available vacancy clusters for capturing neon and forming bubbles are higher in silicon compared to copper [64]. This implies that the subsurface structure induced by Ne ion implantation, and their influence on fracture properties, are highly material-dependent. While Ne ions may not be optimal for notching in silicon without annealing, they could still be effective in other material systems with lower susceptibility to bubble formation.

In summary, the potential of neon ions as a candidate for creating FIB notches in micro cantilever fracture testing was investigated using silicon as a model material. We found that neon ions can mill deep and sharp bridge notches in silicon using a 25 kV acceleration voltage. However, this was at the cost of sub-surface bubbles induced by neon ions. Annealing helped to get a sharp notch front, and a fracture toughness of 1.1 ± 0.1 MPa $m^{0.5}$, which is within the expected range for single crystalline silicon. This demonstrates that neon ions can serve as an alternative option for creating notches in materials where gallium ion-induced artefacts significantly influence fracture properties, thus hindering the use of FIB for producing notches. However, neon ion beams are still not ideal for preparing artefact-free micro fracture samples.

CRediT authorship contribution statement

Eloho Okotete: Writing – original draft, Methodology, Investigation, Formal analysis. **Stefan Mück:** Methodology. **Subin Lee:** Writing – review & editing, Supervision, Methodology, Formal analysis. **Christoph Kirchlechner:** Writing – review & editing, Supervision, Funding acquisition, Formal analysis, Conceptualization.

Declaration of competing interest

The authors declare that they have no known competing financial interests or personal relationships that could have appeared to influence the work reported in this paper.

Acknowledgement

Financial support from the Robert-Bosch-Foundation and from the Helmholtz Program Materials Systems Engineering is gratefully acknowledged. Karlsruhe Nano micro facility (KNMFi) is acknowledged for providing access to the helium ion microscope for this study. C.K. kindly acknowledges the financial support by the European Research Council (ERC) under the grant No. 101043969 (TRITIME).

Supplementary materials

Supplementary material associated with this article can be found, in the online version, at doi:10.1016/j.scriptamat.2024.116509.

Data availability

The data from the work are available under the following DOI: https://doi.org/10.5281/zenodo.14436867.

References

[1] J.P. Best, J. Zechner, J.M. Wheeler, R. Schoeppner, M. Morstein, J. Michler, Small-scale fracture toughness of ceramic thin films: the effects of specimen geometry, ion beam notching and high temperature on chromium nitride toughness evaluation, Philos. Mag. 96 (2016) 3552–3569, https://doi.org/10.1080/14786435.2016.1223891.
[2] G. Dehm, B.N. Jaya, R. Raghavan, C. Kirchlechner, Overview on micro- and nanomechanical testing: new insights in interface plasticity and fracture at small length scales, Acta Mater. 142 (2018) 248–282, https://doi.org/10.1016/j.actamat.2017.06.019.
[3] B.N. Jaya, C. Kirchlechner, G. Dehm, Can microscale fracture tests provide reliable fracture toughness values? A case study in silicon, J. Mater. Res. 30 (2015) 686–698, https://doi.org/10.1557/jmr.2015.2.
[4] S. Wurster, C. Motz, R. Pippan, Characterization of the fracture toughness of micro-sized tungsten single crystal notched specimens, Philos. Mag. 92 (2012) 1803–1825, https://doi.org/10.1080/14786435.2012.658449.
[5] A.D. Norton, S. Falco, N. Young, J. Severs, R.I. Todd, Microcantilever investigation of fracture toughness and subcritical crack growth on the scale of the microstructure in Al_2O_3, J. Eur. Ceram. Soc. 35 (2015) 4521–4533, https://doi.org/10.1016/j.jeurceramsoc.2015.08.023.
[6] L. Borasi, A. Slagter, A. Mortensen, C. Kirchlechner, On the preparation and mechanical testing of nano to micron-scale specimens, Acta Mater. (2024) 120394, https://doi.org/10.1016/j.actamat.2024.120394.
[7] Y. Zhang, M. Bartosik, S. Brinckmann, S. Lee, C. Kirchlechner, Direct observation of crack arrest after bridge notch failure: a strategy to increase statistics and reduce FIB-artifacts in micro-cantilever testing, Mater. Des. 233 (2023) 112188, https://doi.org/10.1016/j.matdes.2023.112188.
[8] E. Okotete, A. Muslija, J. Hohmann, M. Kohl, S. Brinckmann, S. Lee, C. Kirchlechner, Optimisation of bridge notch geometry in single cantilever beams: an approach for minimising FIB artefacts, 2024.
[9] E. Okotete, Stable crack growth geometries as a strategy to circumvent FIB artefacts in small scale fracture testing, Karlsr. Inst. Technol. (KIT) (2024), https://doi.org/10.5445/IR/1000171738.
[10] J.R. Michael, Focused ion beam induced microstructural alterations: texture development, grain growth, and intermetallic formation, Microsc. Microanal. 17 (2011) 386–397, https://doi.org/10.1017/S1431927611000171.
[11] R.C. Hugo, R.G. Hoagland, In-situ TEM observation of aluminum embrittlement by liquid gallium, Scr. Mater. 38 (1998) 523–529, https://doi.org/10.1016/S1359-6462(97)00464-8.
[12] B.A. Benson, R.G. Hoagland, Crack growth behavior of a high strength aluminum alloy during LME by gallium, Scr. Metall. 23 (1989) 1943–1948, https://doi.org/10.1016/0036-9748(89)90487-0.
[13] N. Tsutsui, H. Koizumi, Intergranular /transgranular fracture in the liquid metal embrittlement of polycrystalline embrittlement of polycrystalline zinc, Procedia Struct. Integr. 13 (2018) 849–854, https://doi.org/10.1016/j.prostr.2018.12.162.
[14] J.P. Best, J. Zechner, I. Shorubalko, J.V. Oboňa, J. Wehrs, M. Morstein, J. Michler, A comparison of three different notching ions for small-scale fracture toughness measurement, Scr. Mater. 112 (2016) 71–74, https://doi.org/10.1016/j.scriptamat.2015.09.014.
[15] E.I. Preiß, B. Merle, Y. Xiao, F. Gannott, J.P. Liebig, J.M. Wheeler, M. Göken, Applicability of focused Ion beam (FIB) milling with gallium, neon, and xenon to the fracture toughness characterization of gold thin films, J. Mater. Res. 36 (2021) 2505–2514, https://doi.org/10.1557/s43578-020-00045-w.
[16] E.D. Hintsala, S. Bhowmick, X. Yueyue, R. Ballarini, S.A.S. Asif, W.W. Gerberich, Temperature dependent fracture initiation in microscale silicon, Scr. Mater. 130 (2017) 78–82, https://doi.org/10.1016/j.scriptamat.2016.11.016.
[17] R.F. Cook, Strength and sharp contact fracture of silicon, J. Mater. Sci. 41 (2006) 841–872, https://doi.org/10.1007/s10853-006-6567-y.
[18] S. Tan, R. Livengood, P. Hack, R. Hallstein, D. Shima, J. Notte, S. McVey, Nanomachining with a focused neon beam: a preliminary investigation for semiconductor circuit editing and failure analysis, J. Vac. Sci. Technol. B, Nanotechnol. Microelectron. Mater. Process. Meas. Phenom. 29 (2011), https://doi.org/10.1116/1.3660797.
[19] M.T. Postek, A.E. Vladar, J. Kramar, L.A. Stern, J. Notte, S. McVey, Helium ion microscopy: a new technique for semiconductor metrology and nanotechnology, AIP Conf. Proc. 931 (2007) 161–167, https://doi.org/10.1063/1.2799363.
[20] J. Notte, B. Ward, N. Economou, R. Hill, R. Percival, L. Farkas, S. McVey, An introduction to the helium ion microscope, AIP Conf. Proc. 931 (2007) 489–496, https://doi.org/10.1063/1.2799423.
[21] L. Scipioni, D.C. Ferranti, V.S. Smentkowski, R.A. Potyrailo, Fabrication and initial characterization of ultrahigh aspect ratio vias in gold using the helium ion microscope, J. Vac. Sci. Technol. B, Nanotechnol. Microelectron. Mater. Process. Meas. Phenom. 28 (2010) C6P18–C6P23, https://doi.org/10.1116/1.3517514.
[22] G. Hlawacek, V. Veligura, R. van Gastel, B. Poelsema, Helium ion microscopy, J. Vac. Sci. Technol. B, Nanotechnol. Microelectron. Mater. Process. Meas. Phenom. 32 (2014), https://doi.org/10.1116/1.4863676, 39-1–39-11.
[23] R.H. Livengood, S. Tan, R. Hallstein, J. Notte, S. McVey, F.H.M. Faridur Rahman, The neon gas field ion source—A first characterization of neon nanomachining properties, Nucl. Instrum. Methods Phys. Res. Sect. A Accel. Spectrom., Detect. Assoc. Equip. 645 (2011) 136–140, https://doi.org/10.1016/j.nima.2010.12.220.
[24] S. Tan, R. Livengood, D. Shima, J. Notte, S. McVey, Gas field ion source and liquid metal ion source charged particle material interaction study for semiconductor nanomachining applications, J. Vac. Sci. Technol. B, Nanotechnol. Microelectron. Mater. Process. Meas. Phenom. 28 (2010) C6F15–C6F21, https://doi.org/10.1116/1.3511509.

[25] D. Xia, Y.B. Jiang, J. Notte, D. Runt, GaAs milling with neon focused ion beam: comparison with gallium focused ion beam milling and subsurface damage analysis, Appl. Surf. Sci. 538 (2021), https://doi.org/10.1016/j.apsusc.2020.147922.
[26] K. Matoy, H. Schönherr, T. Detzel, T. Schöberl, R. Pippan, C. Motz, G. Dehm, A comparative micro-cantilever study of the mechanical behavior of silicon based passivation films, Thin Solid Films 518 (2009) 247–256, https://doi.org/10.1016/j.tsf.2009.07.143.
[27] S. Brinckmann, K. Matoy, C. Kirchlechner, G. Dehm, On the influence of microcantilever pre-crack geometries on the apparent fracture toughness of brittle materials, Acta Mater. 136 (2017) 281–287, https://doi.org/10.1016/j.actamat.2017.07.014.
[28] Y. Drezner, Y. Greenzweig, A. Raveh, Strategy for focused ion beam compound material removal for circuit editing, J. Vac. Sci. Technol. B, Nanotechnol. Microelectron. Mater. Process. Meas. Phenom. 30 (2012), https://doi.org/10.1116/1.3674280.
[29] M. Kolíbal, T. Matlocha, T. Vystavěl, T. Šikola, Low energy focused ion beam milling of silicon and germanium nanostructures, Nanotechnology 22 (2011), https://doi.org/10.1088/0957-4484/22/10/105304.
[30] M. Rauscher, E. Plies, Low energy focused ion beam system design, J. Vac. Sci. Technol. A Vac., Surf., Film 24 (2006) 1055–1066, https://doi.org/10.1116/1.2208989.
[31] C.A. Volkert, A.M. Minor, Focused ion beam microscopy and micromachining, MRS Bull. 32 (2007) 389–399, https://doi.org/10.1557/mrs2007.62.
[32] T. Wirtz, P. Philipp, J.N. Audinot, D. Dowsett, S. Eswara, High-resolution high-sensitivity elemental imaging by secondary ion mass spectrometry: from traditional 2D and 3D imaging to correlative microscopy, Nanotechnology 26 (2015), https://doi.org/10.1088/0957-4484/26/43/434001.
[33] H.O. Funsten, S.M. Ritzau, R.W. Harper, J.E. Borovsky, R.E. Johnson, Energy loss by keV ions in silicon, Phys. Rev. Lett. 92 (2004) 2–5, https://doi.org/10.1103/PhysRevLett.92.213201.
[34] L.A. Giannuzzi, B.I. Prenitzer, B.W. Kempshall, Ion - solid interactions, in: F. A. Giannuzzi, L.A. Stevie (Eds.), Introd. to Focus. Ion Beams, Springer US, Boston, MA, 2005, pp. 13–52, https://doi.org/10.1007/0-387-23313-X_2.
[35] T. Wirtz, O. De Castro, J.N. Audinot, P. Philipp, Imaging and analytics on the helium ion microscope, Annu. Rev. Anal. Chem. 12 (2019) 523–543, https://doi.org/10.1146/annurev-anchem-061318-115457.
[36] E. Oliviero, S. Peripolli, P.F.P. Fichtner, L. Amaral, Characterization of neon implantation damage in silicon, Mater. Sci. Eng. B. 112 (2004) 111–115, https://doi.org/10.1016/j.mseb.2004.05.014.
[37] A.G. Cullis, T.E. Seidel, R.L. Meek, Comparative study of annealed neon-, argon-, and krypton-ion implantation damage in silicon, J. Appl. Phys. 49 (1978) 5188–5198, https://doi.org/10.1063/1.324414.
[38] R. Timilsina, S. Tan, R. Livengood, P.D. Rack, Corrigendum: monte Carlo simulations of nanoscale focused neon ion beam sputtering of copper: elucidating resolution limits and sub-surface damage (2014 Nanotechnology 25 485704), Nanotechnology 26 (2015) 119501, https://doi.org/10.1088/0957-4484/26/11/119501.
[39] R. Livengood, S. Tan, Y. Greenzweig, J. Notte, S. McVey, Subsurface damage from helium ions as a function of dose, beam energy, and dose rate, J. Vac. Sci. Technol. B Microelectron. Nanom. Struct. 27 (2009) 3244, https://doi.org/10.1116/1.3237101.
[40] R. Livengood, S. Tan, Y. Greenzweig, J. Notte, S. McVey, Subsurface damage from helium ions as a function of dose, beam energy, and dose rate, J. Vac. Sci. Technol. B Microelectron. Nanom. Struct. Process. Meas. Phenom. 27 (2009) 3244–3249, https://doi.org/10.1116/1.3237101.
[41] R. Li, R. Zhu, S. Chen, C. He, M. Li, J. Zhang, P. Gao, Z. Liao, J. Xu, Study of damage generation induced by focused helium ion beam in silicon, J. Vac. Sci. Technol. B, Nanotechnol. Microelectron. Mater. Process. Meas. Phenom. 37 (2019), https://doi.org/10.1116/1.5096908.
[42] T.C. Pekin, F.I. Allen, A.M. Minor, Evaluation of neon focused ion beam milling for TEM sample preparation, J. Microsc. 264 (2016) 59–63, https://doi.org/10.1111/jmi.12416.
[43] A.C. Eddin, L. Pizzagalli, First-principles calculations of helium and neon desorption from cavities in silicon, J. Phys. Condens. Matter. 24 (2012), https://doi.org/10.1088/0953-8984/24/17/175006.
[44] J. Dérès, M.L. David, K. Alix, C. Hébert, D.T.L. Alexander, L. Pizzagalli, Properties of helium bubbles in covalent systems at the nanoscale: a combined numerical and experimental study, Phys. Rev. B. 96 (2017) 1–12, https://doi.org/10.1103/PhysRevB.96.014110.
[45] S. Peripolli, E. Oliviero, P.F.P. Fichtner, M.A.Z. Vasconcellos, L. Amaral, Characterization of neon cavity in silicon, Nucl. Instrum. Methods Phys. Res. Sect. B Beam Interact. Mater. Atoms. 242 (2006) 494–497, https://doi.org/10.1016/j.nimb.2005.08.138.
[46] Q. Chen, T. Shao, Y. Xing, An experiment-based profile function for the calculation of damage distribution in bulk silicon induced by a helium focused ion beam process, Sensors (Switzerland) 20 (2020), https://doi.org/10.3390/s20082306.
[47] E. Oliviero, S. Peripolli, L. Amaral, P.F.P. Fichtner, M.F. Beaufort, J.F. Barbot, S. E. Donnelly, Damage accumulation in neon implanted silicon, J. Appl. Phys. 100 (2006), https://doi.org/10.1063/1.2220644.
[48] A. Markwitz, V.J. Kennedy, H. Baumann, Formation of micrometer sized crater shaped pits in silicon by low-energy 22Ne+ implantation and electron beam annealing, Nucl. Instrum. Methods Phys. Res. Sect. B Beam Interact. Mater. Atoms. 206 (2003) 179–183, https://doi.org/10.1016/S0168-583X(03)00719-5.
[49] M.G. Stanford, B.B. Lewis, V. Iberi, J.D. Fowlkes, S. Tan, R. Livengood, P.D. Rack, In situ mitigation of subsurface and peripheral focused ion beam damage via simultaneous pulsed laser heating, Small 12 (2016) 1779–1787, https://doi.org/10.1002/smll.201503680.
[50] M.A. Nguyen, M.O. Ruault, F. Fortuna, Formation and growth of nanocavities and cavities induced by He^+ implantation in silicon, Adv. Nat. Sci. Nanosci. Nanotechnol. 3 (2012), https://doi.org/10.1088/2043-6262/3/1/015015.
[51] J.H. Evans, A. Van Veen, C.C. Griffioen, The annealing of helium-induced cavities in silicon and the inhibiting role of oxygen, Nucl. Inst. Methods Phys. Res. B. 28 (1987) 360–363, https://doi.org/10.1016/0168-583X(87)90176-5.
[52] M.F. Beaufort, J.F. Barbot, M. Drouet, S. Peripolli, E. Oliviero, L. Amaral, P.F. P. Fichtner, Nanocavities induced by neon Plasma Based Ion Implantation in silicon, Nucl. Instruments Methods Phys. Res. Sect. B Beam Interact. Mater. Atoms. 257 (2007) 750–752, https://doi.org/10.1016/j.nimb.2007.01.128.
[53] A. Majid, A. Ali, J.J. Zhu, Y.T. Wang, Study of lattice damage produced by neon implantation into AlInN, J. Mater. Sci. Mater. Electron. 20 (2009) 230–233, https://doi.org/10.1007/s10854-008-9708-z.
[54] B.N. Jaya, J.M. Wheeler, J. Wehrs, J.P. Best, R. Soler, J. Michler, C. Kirchlechner, G. Dehm, Microscale fracture behavior of single crystal silicon beams at elevated temperatures, Nano Lett. 16 (2016) 7597–7603, https://doi.org/10.1021/acs.nanolett.6b03461.
[55] M. Brede, P. Haasen, The brittle-to-ductile transition in doped silicon as a model substance, Acta Metall. 36 (1988) 2003–2018, https://doi.org/10.1016/0001-6160(88)90302-1.
[56] C. St. John, The brittle-to-ductile transition in pre-cleaved silicon single crystals, Philos. Mag. 32 (1975) 1193–1212, https://doi.org/10.1080/14786437508228099.
[57] R.J. Jaccodine, Surface energy of germanium and silicon, J. Electrochem. Soc. 110 (1963) 524, https://doi.org/10.1149/1.2425806.
[58] F.W. DelRio, R.F. Cook, B.L. Boyce, Fracture strength of micro- and nano-scale silicon components, Appl. Phys. Rev. 2 (2015), https://doi.org/10.1063/1.4919540.
[59] P.B. Hirsch, S.G. Roberts, The brittle-ductile transition in silicon, Philos. Mag. A Phys. Condens. Matter, Struct. Defects Mech. Prop. 64 (1991) 55–80, https://doi.org/10.1080/01418619108206126.
[60] C. Chen, M. Leipold, Fracture toughness of silicon, Am. Ceram. Soc. Bull. 59 (1980) 469–473.
[61] D. Di Maio, S.G. Roberts, Measuring fracture toughness of coatings using focused-ion-beam-machined microbeams, J. Mater. Res. 20 (2005) 299–302, https://doi.org/10.1557/JMR.2005.0048.
[62] M.G. Mueller, G. Žagar, A. Mortensen, Stable room-temperature micron-scale crack growth in single-crystalline silicon, J. Mater. Res. 32 (2017) 3617–3626, https://doi.org/10.1557/jmr.2017.238.
[63] F.H.M. Rahman, S. McVey, L. Farkas, J.A. Notte, S. Tan, R.H. Livengood, The prospects of a subnanometer focused neon ion beam, Scanning 34 (2012) 129–134, https://doi.org/10.1002/sca.20268.
[64] C.A. Cima, H. Boudinov, J.P. De Souza, Y. Suprun-Belevich, P.F.P. Fichtner, Strain development and damage accumulation during neon ion implantation into silicon at elevated temperatures, J. Appl. Phys. 88 (2000) 1771–1775, https://doi.org/10.1063/1.1305928.